Available online at www.sciencedirect.com
SCIENCE DIRECT®
Journal of the European Ceramic Society 25 (2005) 3293–3299
www.elsevier.com/locate/jeurceramsoc

Statistical simulation of microcrack toughening in advanced ceramics

C.K. Chen*

Department of Mechanical Engineering, Cheng Shiu University Neausong 833, Kaohsiung, Taiwan

Received 31 March 2004; received in revised form 29 July 2004; accepted 15 August 2004

Abstract

A statistical distribution of microcracks is simulated as a damage process zone developed around the vicinity of a macro-crack in a brittle ceramic. Uniform distributions of microcrack location and orientation are assumed in a Monte Carlo process to represent isotropic damage. An alternating iteration numerical technique is employed to evaluate the main-crack and the damage zone microcracks interactions, and the behavior of the main-crack either in shielding or anti-shielding modes may then be assessed. With the assumption of dilute microcrack concentration, however, one can neglect the microcrack–microcrack interaction, and the interacting stress intensity factor (SIF) at the main-crack tip can then be superimposed for each microcrack. In this study, two general sources of loading are evaluated, one is for the main-crack microcrack interaction under an applied remote load, and the other is for the main-crack microcrack interaction accompanied by the relief of residual stresses on the microcrack surfaces. Nevertheless, the results show that these two conditions together with the isotropic damage assumption can always shield the main-crack tip, and therefore increase the ceramic toughness. In addition, it is found that microcracks behind the main-crack tip can make the most shielding whereas microcracks ahead of the main-crack tip play no role in shielding.

Keywords: Toughness and toughening; Fracture; Defects; Statistical model; Modeling

1. Introduction

Experimental evidence shows that advanced ceramics can have high macroscopic fracture toughness many times greater than the fracture energy for cleavage of their grains or for separating their grain boundaries. Thus several toughening micro-mechanisms have been suggested to account for this phenomenon. Theses proposing toughening mechanisms are concerned with the heterogeneity in the micro-scale properties, such as at the grain level. One general consideration is micro-obstacles in the crack growth path; such that pinning of the crack results in toughening owing to crack bowing, tilting, twisting and bridging,[1–3] or more generally crack deflection. In addition, phase transformation such as the martensitic phase transformation in zirconia-toughened alumina, can provide transformation dilatation to toughen the ceramics.[4] Another consideration in ceramic toughening mechanisms is the possibility of micro-crack formation in the fracture process zone[5,6] that may shield the main-crack and then toughen the ceramics. These microcracks can be created as a combined effect of externally applied loads and localized residual stresses, where residual stresses are generated by thermal expansion anisotropy in single-phase ceramics or elastic mismatch in multi-phase ceramics.

Microcrack toughening is mainly attributed to two potential sources.[4] One is the main-crack and microcrack interaction that causes stress redistribution ahead of the main-crack tip and thus lowers the continuum stiffness of the microcracked material. The other contribution is the stress redistribution at the main-crack tip due to the release of residual stress when a microcrack is nucleated. In the literature, there are two different approaches to modeling the microcracking damage, namely continuum damage and discrete damage. The first concept considers a damage zone with reduced effective moduli, and attention is focused on the derivation of the constitutive governing relation of this damaged solid.[7,8] However, the other approach adopts discrete

* Fax: +886 7 7337100.
E-mail address: joss@csu.edu.tw.

0955-2219/$ – see front matter © 2004 Elsevier Ltd. All rights reserved.
doi:10.1016/j.jeurceramsoc.2004.08.017

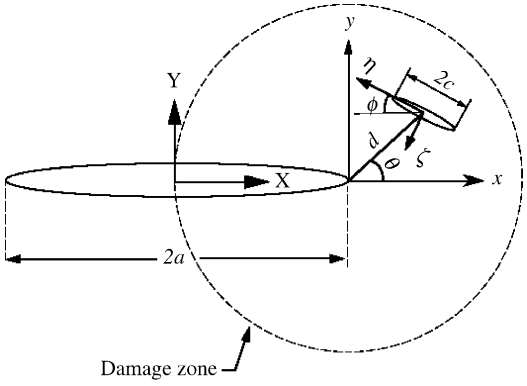

Fig. 1. Schematic representation of main-crack and a micro-crack in the circular damage zone.

micro-mechanics to model the damage zone where the microcrack is treated as an individual identity. The interacting effects among these microcracks and the main-crack are calculated, and then an average scheme is applied to approximate the overall damage.[4,9–11] Nevertheless, these two different approaches, to a certain extent, do not lead to the same conclusions.[4,8]

The discrete approach is applied to evaluate the extent of micro-crack toughening in this presentation. The microcrack damage zone, in the literature, is proposed to be a near-tip fracture process zone[12,13] where microcracks are generated. This approach is based on the remote load intensity and a microcrack precursor nucleation assumption, and therefore analytical expressions can be derived for the size and shape of this process zone. Nevertheless, considering the actual granular microstructure of microcracking materials suggest that microcracks are grain-facet sized, located and oriented. Inherently random distributions of grain facets are recognized and then formation of microcracks yields microstructure disorder. In addition, microcracks may be initiated in the ceramic hot-pressing process and are not limited to the presence of applied loads. In the study, a microcracking damage zone is assumed to be a circular zone situated around the main-crack tip, as shown in Fig. 1. Locations and orientations of microcracks are randomly placed with employment of the Monte Carlo technique, and the statistical effect at the main-crack tip for various damage zones can then be evaluated.

2. Alternating iteration in cracks interaction

A discrete model of an arbitrary located and oriented micro-crack near the main-crack tip with remote loading K_{I}^{∞} is first analyzed, where $K_{\mathrm{I}}^{\infty} = \sigma^{\infty}\sqrt{\pi a}$ and σ^{∞} denotes a remote load which is shown in Fig. 2(a), where $c = a/20$, as can be reasonably simulated for the microcrack behavior. As follows in the notation used in this article, X, Y denote the coordinate axes with origin at the center of the main-crack and x, y represent the main-crack tip coordinate, whereas, η and ς are coordinates observed from the center of the microcrack.

In the frame of linear-elastic fracture mechanics, the problem is decomposed into two sub-problems, as illustrated in Fig. 2. To depict the influence of residual stresses in the brittle material, the residual stresses σ_{Res} and τ_{Res} are assumed to prevail uniformly along the microcrack surface. Fig. 2(a) can be further decomposed by the principle of Büeckner's superposition, which is demonstrated in Fig. 3, and the surface tractions on both main-crack and micro-crack are derived as

$$p_{\mathrm{MAIN}}^{0} = \sigma^{\infty} = \frac{K_{\mathrm{I}}^{\infty}}{\sqrt{\pi a}}, \quad q_{\mathrm{MAIN}}^{0} = 0 \tag{1}$$

$$p_{\mathrm{MIC}}^{0} = \frac{K_{\mathrm{I}}^{\infty}}{\sqrt{\pi c}}\cos^{2}\theta, \quad q_{\mathrm{MIC}}^{0} = \frac{K_{\mathrm{I}}^{\infty}}{\sqrt{\pi c}}\sin\theta\cos\theta \tag{2}$$

Two potential shielding sources are modeled in Fig. 2(b) and Fig. 2(c) respectively. Fig. 2(b) is to account for the elastic interaction of cracks, and that of Fig. 2(b) is attributed to the relief of residual stresses. Two sub-problems of Fig. 3(c) and Fig. 2(c) can now be appropriately solved by an alternating iteration method[14,15] and are thus resolved respectively to free its own crack surface tractions. In each loading system, stress distributions on the imaginary position of cracks are calculated with corresponding Westergaard stress functions.[16]

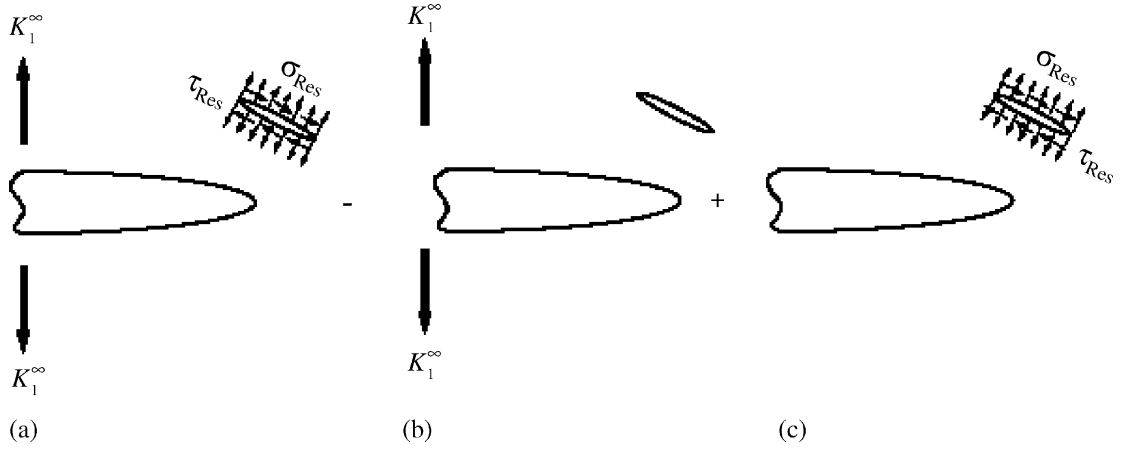

Fig. 2. Elastic decomposition of remote loading and residual stresses.

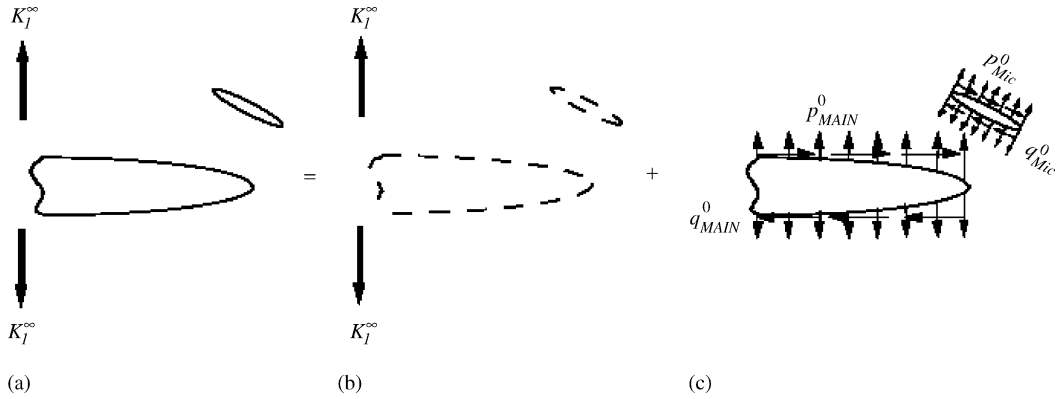

Fig. 3. Decomposition in Büeckner's superposition in a cracked solid.

Whereas only one crack exists in each iterating cycle, the remaining crack is considered as an imaginary crack. For numerical convenience, constant tractions on imaginary positions are averaged along each crack length. Distributed stresses shed on the domain are thus derived approximately from these constant tractions. The stress field with negative traction on each imaginary crack is then imposed onto the existing stress field to free crack surface traction. In doing so, new image traction may be introduced to the original image traction free crack. These remaining image tractions are successively reduced by the repeated alternating iteration. A similar process is repeated until the remaining image tractions on both cracks approach zero simultaneously. There is an obvious advantage to this iteration method, in which the interaction effect between cracks has been considered. The imaginary traction on the free surfaces of a prospective crack can then be imposed in every iteration cycle. Therefore, the kth increment of stress intensity factors (SIF) at main-crack tip ($\Delta K^k_{\mathrm{MAIN}}(\pm a)$) owing to mutual crack interaction can be integrated from the concentrated force results provided in Tada et al.[16] and displayed in Eq. (3), where $p^k_{\mathrm{MAIN}}(X)$ and $p^k_{\mathrm{MAIN}}(X)$ are the normal and shear image stress functions distributed along the main-crack in the kth iteration.

$$\Delta K^k_{\mathrm{I,MAIN}}(\pm a) = \frac{1}{\sqrt{\pi a}} \int_{-a}^{a} p^k_{\mathrm{MAIN}}(X) \sqrt{\frac{a \pm X}{a \mp X}}\, \mathrm{d}X$$
$$\Delta K^k_{\mathrm{II,MAIN}}(\pm a) = \frac{1}{\sqrt{\pi a}} \int_{-a}^{a} q^k_{\mathrm{MAIN}}(X) \sqrt{\frac{a \pm X}{a \mp X}}\, \mathrm{d}X \quad (3)$$

The induced stress intensity factors (ΔK_{I}, ΔK_{II}) owing to the presence of a microcrack can then be superposed for every iteration cycle k.

3. Statistical experiments

In this investigation, microcrack initiation and growing are not addressed and the damage zone is considered plainly to be a circular one. To demonstrate the extent of disorder in the microstructure, the microcrack size, location and orientation are governed by the heterogeneity of microstructure grain boundaries. With good efficiency in convergence of alternating iteration, statistical stability at the main-crack tip may be calculated and superimposed for every randomly distributed microcrack in a damage zone.

3.1. Microcrack distribution

Microcrack density[17] in two-dimensions can be evaluated in terms of a characteristic area A containing N_A microcracks of characteristic length $2c$, i.e.,

$$\rho = \frac{1}{A} N_A (2c)^2$$

It is found experimentally in Rühle et al.[6] and Han et al.[18] that the microcrack density in alumina-zirconia is between 0.00 and 0.24 and in silicon–carbide alloy is 0.31–0.47. In the assumption of a dilute concentration of microcrack, interactions among microcracks are neglected. However, it is noted in reference[13] that crack interaction is not such a short-range effect as sometimes expected. Hence, the average measure of microcracking damage zone size (A) in the vicinity of a main-crack tip is assumed to be in the circular zone with radius of half main-crack length, i.e., $A = \pi a^2$. In this study, various crack densities are exhibited in the microcracking damage zone having 30, 50, 80 and 100 microcracks, where microcrack density (ρ) is 0.096, 0.159, 0.255 and 0.318 correspondingly.

In considering the actual granular microstructure of advance ceramics, it can be considered that microcracks are grain-facet sized, located and oriented. Therefore, microcrack length is kept constant at $a/20$ and the location and orientation can be varied with arbitrarily chosen geometric parameters (d, θ, ϕ), as illustrated in Fig. 1. Uniformly distributed geometric variables can result in maximum scattering in microcracks, and statistical disorder in microcracks can be retained as for grain boundaries. Hence, microcracking damage can be regard as isotropic with the assumption of uniform distributions. The statistical distribution functions have been simulated by means of Monte Carlo techniques, and geometric parameters are uniformly distributed

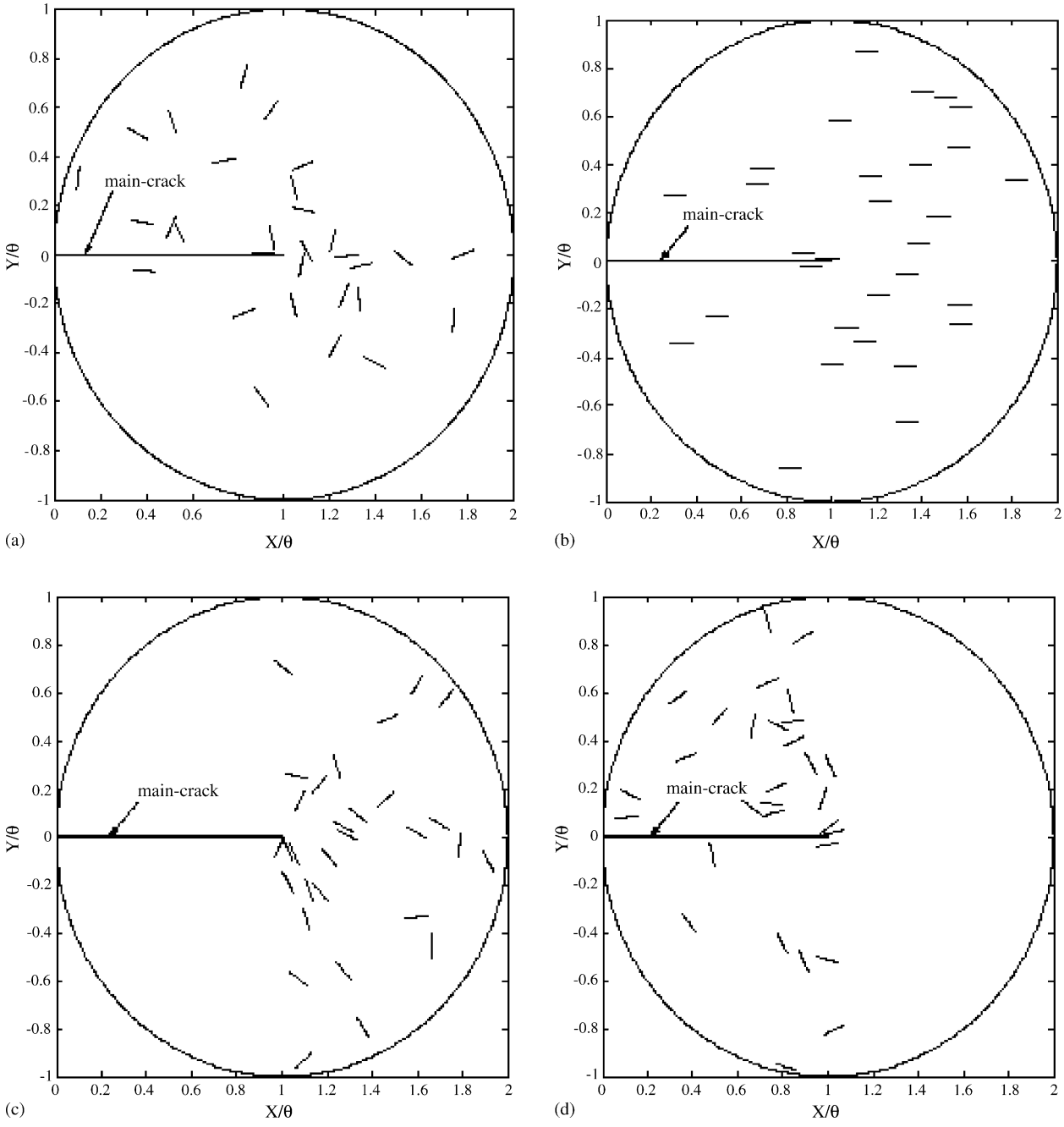

Fig. 4. One example of 30 microcracks distributed in the circular damage zone (a) around the crack tip; (b) parallel the crack-tip; (c) ahead the crack-tip; (d) behind the crack-tip.

in the range of $-a \le d \le a$, $-\pi < \theta < \pi$ and $0 \le \phi \le 2\pi$. One hundred specimens for each crack density are tested and averaged to evaluate the statistically stable stress intensity factor at the main-crack tip. In addition, main-micro and microcrack–microcrack intersections are excluded in this Monte Carlo simulation.

3.2. Simulation of damage zone

Four different kinds of damage zones are evaluated in the Monte Carlo simulation. A group of 100 specified damage zones is employed as a statistical population for each crack density. The microcracking damage zone around the main-crack tip ($0 < d \le a$, $-\pi < \theta < \pi$, $0 \le \phi \le 2\pi$) is attributed to the isotropic damage in the material, as illustrated in Fig. 4(a) and denoted as case A. Case B is shown in Fig. 4(b) for parallel microcrack damage around the main-crack ($0 < d \le a$, $-\pi < \theta < \pi$, $\phi = 0$). It is for the comparison of the influence of an anisotropic microcracking damage case. Furthermore, in Fig. 4(c) and (d), designated cases C and D correspondingly, assessment is made for distributed microcracking zones in front of the main-crack tip ($0 < d \le a$, $-\pi/2 \le$

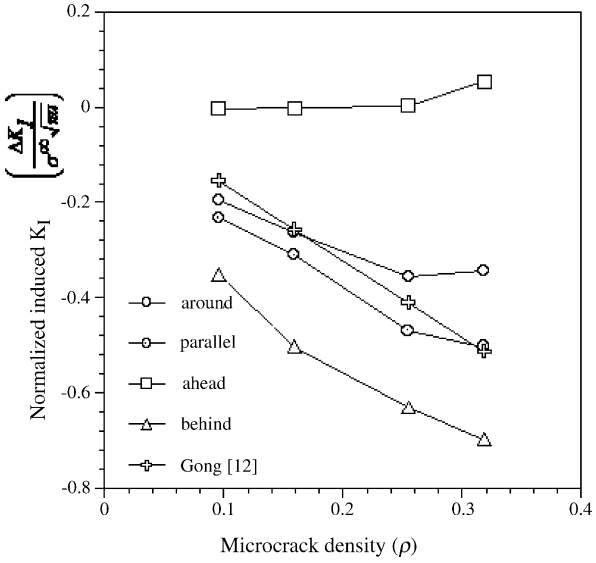

Fig. 5. The normalized induced mode I stress intensity factor at main-crack tip for different microcrack density and damage zones.

$\theta \le \pi/2, 0 \le \phi \le 2\pi$) and behind the main-crack tip ($0 < d \le a, \pi/2 \le \theta \le 3\pi/2, 0 \le \phi \le 2\pi$). These situations are evaluated to assess the shielding degree of isotropic damage in a microcrack annular zone surrounding the main-crack tip.

In the evaluation of the first shielding source from the elastic interaction, the resulting statistical consequence for ΔK_I at the main-crack tip can be examined in Fig. 5. However, random microcracks may result in an anti-symmetric stress field and ΔK_{II} can arise as depicted in Fig. 6. Investigating Fig. 5 shows that a shielding effect prevails for cases A, B and D and increases with increasing crack density. However, crack density must be retained in a reasonable range for the assumption of dilute concentration to be valid. In case A, microcracking toughening is attained; it relates closely to the conclusion of

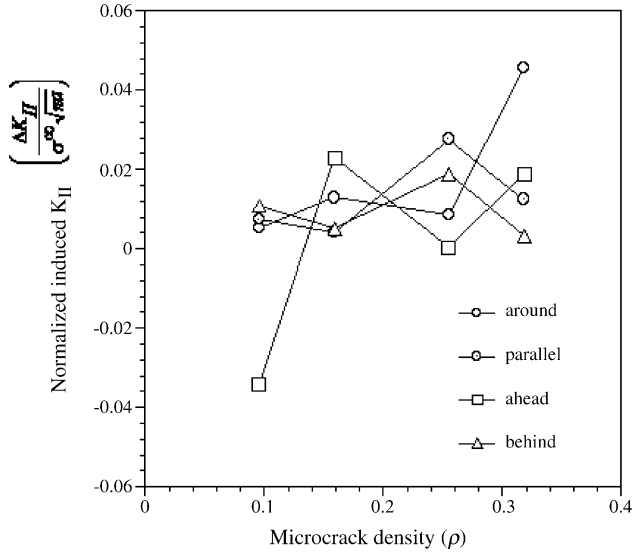

Fig. 6. The normalized induced mode II stress intensity factor at main-crack tip for different microcrack density and damage zones.

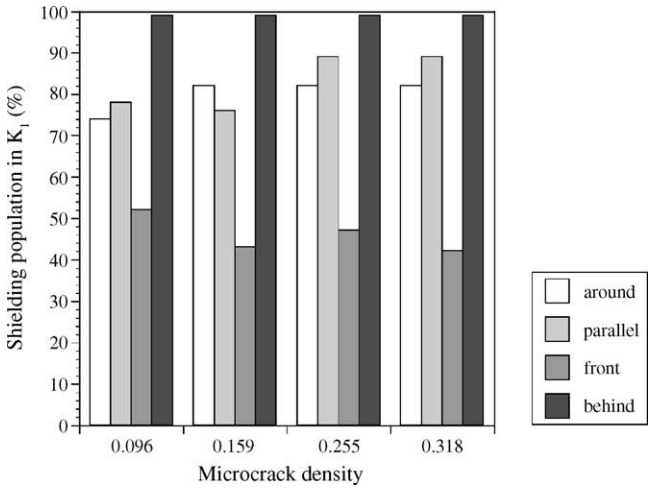

Fig. 7. Shielding populations in K_I for different microcrack density and damage zones.

Gong[12] for small crack density. Gong[12] estimated the shielding as $\Delta K = -1.61\rho K_I^{\infty}$ for a stationary main-crack even though its approach is quite dissimilar to this model. In case B, anisotropic damage may enhance the shielding effect in comparison with the isotropic case A. Nevertheless, a microcracking zone behind the crack tip provides the greatest shielding effect while one ahead of the main-crack tip can contribute little or no effect on microcrack toughening.

The induced mode II stress intensity factor for any case are small compared to mode I, and lie within the range of ±5%, as observed in Fig. 6. The population in shielding can be examined in Fig. 7. Almost 100% of shielding is in case D and about 50% in case C. This statistical approach is similar to that of Montagut and Kachanov[19] but differences exist,

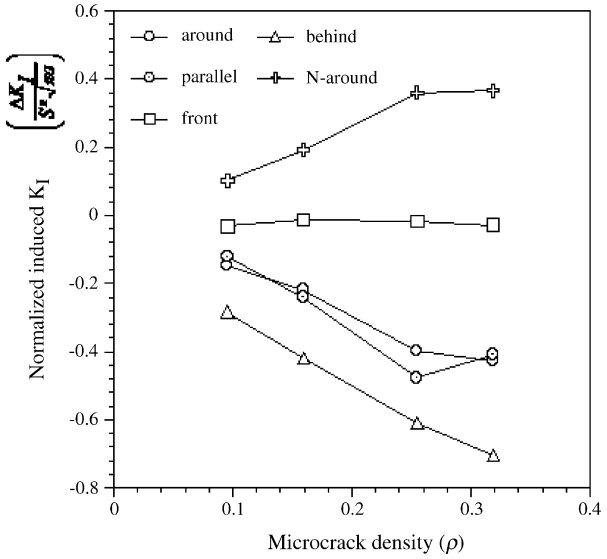

Fig. 8. The residual stresses induced normalized induced mode I stress intensity factor at main-crack tip for different microcrack density and damage zones.

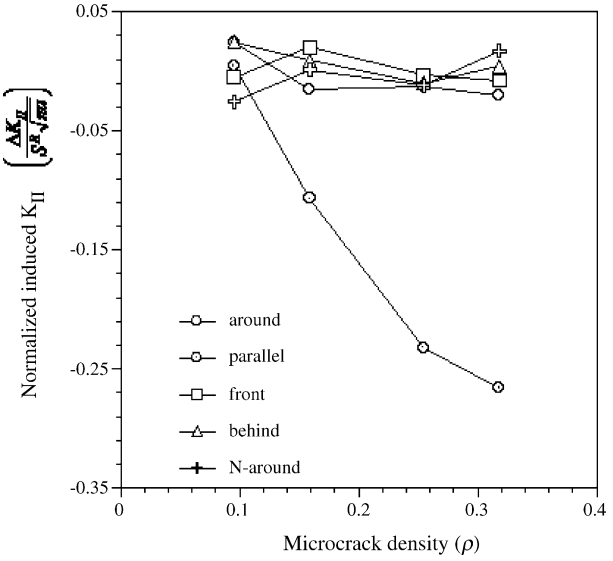

Fig. 9. The residual stresses induced normalized induced mode II stress intensity factor at main-crack tip for different microcrack density and damage zones.

however, a statistical population limited to six coupons,[19] is not enough to get a stable result.

For the second shielding source of interaction problem, the uniform residual stress relieved at the microcrack is denoted as $\sigma_{Res} = \tau_{Res} = S^R$ Similar trends are obtained and depicted in Fig. 8, but the shielding effect is not so prominent as that illustrated in Fig. 5. For the isotropic damage demonstrated in case A, the residual stress relief induced shielding phenomena persisted in contrast to the one of Gong and Meguid[20] where no shielding arose. However, for the damage zone in case C, there is nearly no shielding effect; the case D gets the greatest shielding. A special case of $\sigma_{Res} = -S^R$, $\tau_{Res} = S^R$ is denoted in Fig. 8 as N-around, where anti-shielding is recognized and the compressive residual normal stress produces amplification in ΔK_I.

The induced mode II SIF are confined in the range of ±5% for cases of A, C, D as shown in Fig. 9, but the anisotropic case of parallel microcracks (case B) results in a large deviation of mode II SIF. In the assessment of ceramic toughness in such a case, one cannot ignore the effect of mode II and an equivalent stress intensity factor (K_{eq}) formulation must be involved. The shielding population in ΔK_I is shown in Fig. 10, a similar result to that obtained in Fig. 7.

4. Concluding remarks

Up to 3600 numerically simulated microcrack damage zones are simulated in the circular zone around the main-crack tip. Uniform distribution functions developed with the Monte Carlo technique can place microcracks sufficiently randomly as to represent of microstructure disorder. Two shielding sources in main-crack and microcrack interactions are evaluated statistically. The following conclusions can be drawn:

(1) The alternating iteration method can estimate the main-micro crack interaction efficiently and accurately, making the statistical assessment possible.
(2) Two shielding sources are proved to enhance ceramic toughness with the assumption of isotropic damage, where consistent results exist for this discrete model and for a continuum model.[8]
(3) Microcracks behind the main-crack tip provide the most shielding; no shielding effect is contributed from microcracks situated ahead of the main-crack tip.

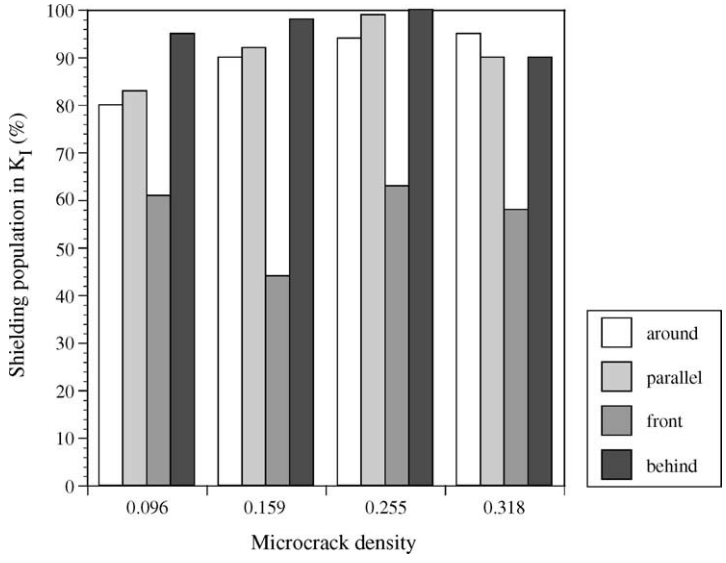

Fig. 10. Shielding populations of residual stress induced K_I for different microcrack density and damage zones.

(4) An anisotropic damage zone may shield mode I SIF at the main-crack tip more than an isotropic one for the first source; however, shielding from residual stress relief (second source) can make mode II significant.
(5) Compressive normal residual stress may produce an anti-shielding effect at the main-crack tip, it should be noted for the design of advanced ceramic materials.

Acknowledgement

The author wishes to express his thanks to the support of Taiwan National Science Council under the grant of 92-2216-E-230-004.

References

1. Evans, A. G., The strength of brittle materials containing second phase dispersions. *Phil. Mag.*, 1972, **26**, 1327–1344.
2. Faber, K. T. and Evans, A. G., Crack deflection processes. I. Theory. *Acta Metall.*, 1983, **31**, 565–576.
3. Faber, K. T. and Evans, A. G., Crack deflection processes. II. Experiments. *Acta Metall.*, 1983, **3**, 577–584.
4. Hutchinson, J. W., Crack tip shielding by micro-cracking in brittle solids. *Acta Metall.*, 1987, **35**, 1605–1619.
5. Claussen, N., Steeb, J. and Pabst, R. B., Effect of induced microcracking in the fracture toughness of ceramics. *Bull. Am. Ceram. Soc.*, 1977, **56**, 559–562.
6. Rühle, M., Evans, A. G., McMeeking, R. M., Charalambides, P. G. and Hutchinson, J. W., Microcrack toughening in alumina/zirconia. *Acta Metall.*, 1987, **35**, 1701–1710.
7. Evans, A. G. and Faber, K. T., Crack-growth resistance of microcracking brittle materials. *J. Am. Ceram. Soc.*, 1984, **6**, 255–260.
8. Oritz, M., Continuum theory of crack shielding in ceramic. *J. App. Mech.*, 1987, **54**, 54–58.
9. Kachanov, M., Elastic solids with many cracks: a simple method of analysis. *Int. J. Solids Struct.*, 1987, **23**, 23–43.
10. Hori, M. and Nemat-Nasser, S., Interacting micro-cracks near the tip in the process zone of a macro-crack. *J. Mech. Phys. Solids*, 1987, **35**, 601–629.
11. Gong, S. X. and Meguid, S. A., Microdefect interaction with a main crack: a general treatment. *Int. J. Mech. Sci.*, 1992, **34**, 933–945.
12. Gong, S. X., On the formation of near-tip microcracking and associated toughening effects. *Eng. Frac. Mech.*, 1995, **50**, 29–39.
13. Brencich, A. and Carpinteri, A., Stress field interaction and strain energy distribution between a stationary main crack and its process zone. *Eng. Frac. Mech.*, 1998, **59**, 797–814.
14. Kuang, J. H. and Chen, C. K., Alternating iteration method for interacting multiple crack problems. *Fatigue Fract. Mater. Struct.*, 1998, **21**, 743–752.
15. Cai, H. and Faber, K. T., On the use of approximation method for microcrack shielding problems. *ASME J. Appl. Mech.*, 1992, **59**, 479–501.
16. Tada, H., Paris, P. C. and Irwin, G. R., *The Stress Analysis of Cracks Handbook*. Paris Productions Incorporated (and Del Research Corporation), Paris, 1985.
17. Kachanov, M., Elastic solids with many cracks and related problems. *Adv. Appl. Mech.*, 1993, **30**, 259–445.
18. Han, L. X. and Suresh, S., High-temperature failure of an alumina–silicon carbide composite under cyclic loads: mechanism of fatigue crack tip damage. *J. Am. Ceram. Soc.*, 1989, **72**, 1233–1238.
19. Montagut, M. and Kachanov, M., On modeling a microcracked zone by weakened elastic material and on statistical aspects of crack–microcrack interactions. *Int. J. Fracture*, 1988, **37**, R55–R62.
20. Gong, S. X. and Meguid, S. A., On the effect of the release of residual stresses due to near-tip microcracking. *Int. J. Fracture*, 1991, **52**, 257–274.